

# Fermi Surface of RuO<sub>2</sub> Measured by Quantum Oscillations

Zheyu Wu<sup>1</sup>, Mengmeng Long<sup>1</sup>, Hanyi Chen<sup>1</sup>, Shubhankar Paul<sup>2,3</sup>, Hisakazu Matsuki<sup>2</sup>, Oleksandr Zheliuk<sup>4</sup>, Uli Zeitler<sup>4</sup>, Gang Li<sup>5,6</sup>, Rui Zhou<sup>5,6</sup>, Zengwei Zhu<sup>7</sup>, Dave Graf<sup>8</sup>, Theodore I. Weinberger<sup>1</sup>, F. Malte Grosche<sup>1</sup>, Yoshiteru Maeno<sup>2,\*</sup> and Alexander G. Eaton<sup>1,†</sup>

<sup>1</sup>*Cavendish Laboratory, University of Cambridge, JJ Thomson Avenue, Cambridge, CB3 0HE, United Kingdom*

<sup>2</sup>*Toyota Riken-Kyoto University Research Center (TRiKUC), Kyoto University, Kyoto 606-8501, Japan*

<sup>3</sup>*Department of Physics, Indian Institute of Technology Kanpur, Kanpur 208016, India*


<sup>4</sup>*High Field Magnet Laboratory (HFML-EMFL), Radboud University, Toernooiveld 7, 6525 ED Nijmegen, The Netherlands*

<sup>5</sup>*Beijing National Laboratory for Condensed Matter Physics, Institute of Physics, Chinese Academy of Sciences, Beijing 100190, China*

<sup>6</sup>*School of Physical Sciences, University of Chinese Academy of Sciences, Beijing 100190, China*

<sup>7</sup>*Wuhan National High Magnetic Field Center and School of Physics, Huazhong University of Science and Technology, Wuhan 430074, China*

<sup>8</sup>*National High Magnetic Field Laboratory, Tallahassee, Florida, 32310 USA*

 (Received 8 April 2025; revised 13 June 2025; accepted 10 July 2025; published 18 August 2025)

The metallic oxide RuO<sub>2</sub> has emerged as a promising altermagnet candidate, owing to reports of this material hosting antiferromagnetic ordering accompanied by a spin-split electronic band structure characteristic of time-reversal symmetry breaking. However, recent studies have robustly questioned this scenario. Here we map the Fermi surface of pristine single-crystalline RuO<sub>2</sub>. By measuring magnetic quantum oscillations of a bulk thermodynamic property, our study resolves the electronic structure present in the bulk of RuO<sub>2</sub>. Several Fermi sheets are discerned, with a range of effective quasiparticle masses up to 5 times that of the bare electron mass. We compare our measurements with the predictions for altermagnetic and nonmagnetic Fermi surfaces deduced from density functional theory calculations. The quantum oscillatory frequency spectra correspond very poorly to the profile expected for the case of altermagnetism; by contrast, they correspond well to the nonmagnetic scenario. Our findings place significant constraints on the bulk magnetic properties of RuO<sub>2</sub> and strongly suggest that this material is an itinerant electron paramagnet.

DOI: [10.1103/PhysRevX.15.031044](https://doi.org/10.1103/PhysRevX.15.031044)

Subject Areas: Condensed Matter Physics, Magnetism

## I. INTRODUCTION

The recently proposed phenomenon of an altermagnetic (AM) phase of matter—characterized by a compensated collinear magnetic structure with a spin polarization that alternates through both the crystal structure in real space and the electronic band structure in reciprocal space—has attracted widespread attention [1–10]. In addition to being of great fundamental interest—constituting a novel, distinct class of magnetic order—there are numerous properties of AM materials that make them highly desirable for

technological applications [11,12]. For example, their time-reversal symmetry-broken electronic band structures may, as per ferromagnetic materials, manifest spin-polarized currents accompanied by the anomalous Hall effect [3,4]. Furthermore, attempts to miniaturize ferromagnetic components within integrated circuits often suffer deleterious effects from stray fields causing interference between neighboring elements. By contrast, the lack of a net magnetization **M** for AM components could enable them to be spatially positioned much closer together in next-generation spintronic circuitry.

Several materials have been theoretically predicted to exhibit AM ordering [6,8]. Among these, the rutile compound RuO<sub>2</sub> quickly emerged as an especially promising candidate [3,8]. Antiferromagnetic ordering in this material was inferred from measurements of neutron diffraction [13] and x-ray scattering [14], with these experiments interpreted to indicate the presence of compensated magnetic moments aligned along the rutile *c* axis. Several predicted

\*Contact author: maeno.yoshiteru.b04@kyoto-u.jp

†Contact author: alex.eaton@phy.cam.ac.uk

Published by the American Physical Society under the terms of the [Creative Commons Attribution 4.0 International license](https://creativecommons.org/licenses/by/4.0/). Further distribution of this work must maintain attribution to the author(s) and the published article's title, journal citation, and DOI.

AM properties were reported from subsequent experimental studies, including observations of the anomalous Hall effect [15], spin-current generation [16–19] along with magnetic circular dichroism indicative of time-reversal symmetry breaking in the band structure [20].

However, the widely held interpretation of  $\text{RuO}_2$  being an archetypical altermagnet has recently been strongly challenged. Firstly, muon spin rotation measurements were unable to detect any signatures of magnetic ordering down to a detection limit of  $<1 \times 10^{-3} \mu_B$  per Ru site, where  $\mu_B$  is the Bohr magneton [21,22]. Secondly, while some photoemission experiments were interpreted to have resolved a  $d$ -wave spin pattern characteristic of AM ordering [20,23], subsequent photoemission studies reported no evidence of AM spin splitting in the band structure [24,25]. Instead, heavy surface states were identified, of a possible topological origin. A Rashba-like spin splitting at the surface was also reported [24], which may explain the observation of magnetic circular dichroism [20]. Given this controversy between surface-sensitive studies, a clear unambiguous determination of the bulk electronic band structure of  $\text{RuO}_2$  is therefore urgently required to shed light on the intrinsic electronic and magnetic properties of this material.

Here we report de Haas–van Alphen (dHvA) and Shubnikov–de Haas (SdH) effect measurements of quantum oscillations (QOs) [26] in the magnetic torque and contactless resistivity of pristine quality single-crystal  $\text{RuO}_2$ . QO measurements have been proposed as an ideal diagnostic tool for probing altermagnet candidates, due to this technique’s high fidelity for resolving the spin splitting of electronic bands such materials must necessarily possess [27]. We measured the evolution in QO frequency upon rotating the orientation of applied magnetic field  $\mathbf{H}$  between the [001]-[100] and [100]-[010] crystallographic axes, to probe the geometrical and topological properties of the  $\text{RuO}_2$  Fermi surface. We compare our experimental observations with theoretical calculations, and find our measurements to be very well described by  $\text{RuO}_2$  being a paramagnetic metal possessing no magnetic ordering.

## II. EXPERIMENTAL TECHNIQUES

Single crystals of  $\text{RuO}_2$  used in this study were grown by the vapor-transport method in flowing oxygen. The details of the growth condition are described in Ref. [28], with most of the crystals used in this study coming from the same crystal growth batch as that used in a recent photoemission study [25]. Temperature dependence of the electrical resistivity shows metallic behavior with a residual resistivity of  $0.1 \mu\Omega \text{ cm}$  for current along the [001] direction, with a residual resistivity ratio of 400, indicative of pristine sample quality.

We performed measurements in four separate magnet systems. Capacitive torque magnetometry experiments were undertaken in steady magnetic fields up to 31 T in a resistive magnet at the High Field Magnet Laboratory (HFML-EMFL), Nijmegen, The Netherlands and up to 30 T in a superconducting magnet at the Synergetic Extreme Condition User Facility (SECUF), Beijing, China. The HFML-EMFL magnet was fitted with a  $^3\text{He}$  sample environment attaining a base temperature of 0.4 K, while in SECUF we utilized a dilution refrigerator enabling temperatures as low as 60 mK. We also measured the contactless resistivity of  $\text{RuO}_2$  by the tunnel diode oscillator (TDO) and proximity detector oscillator (PDO) techniques [29,30]. TDO measurements were performed at SECUF and at the National High Magnetic Field Laboratory (NHMFL), Florida, in a resistive magnet attaining 41.5 T at a base temperature of 0.4 K. PDO measurements were taken at the Wuhan National High Magnetic Field Center (WNHMFC), Wuhan, China. Our PDO experiments were performed in a pulsed magnet reaching a maximum field strength of 57 T, at a base temperature of 0.7 K.

For torque magnetometry measurements, samples were aligned by Laue diffractometry and affixed to a BeCu cantilever using a low-temperature adhesive varnish. This technique constitutes a bulk-sensitive thermodynamic measurement that provides a highly sensitive probe of the anisotropy in a material’s magnetic susceptibility tensor. Because of its high resolution, torque magnetometry is often deployed for dHvA effect measurements in high magnetic fields [31–34]. In HFML-EMFL the magnetic torque  $\tau = \mu_0(\mathbf{M} \times \mathbf{H})$  was measured capacitively by a general radio analog capacitance bridge, and calibrated to absolute units using an Andeen-Hagerling (AH) digital capacitance bridge. At SECUF, we measured  $\tau$  directly with an AH bridge. In both sets of torque experiments, samples were rotated *in situ*, with the orientation calibrated by a Hall sensor. For contactless resistivity measurements, samples were also aligned by Laue diffractometry and affixed to hand-wound copper coils by low-temperature adhesive varnish. TDO and PDO measurements were obtained utilizing a similar methodology to that outlined in Ref. [35]. At WHMFC, samples were also rotated *in situ*, with the orientation determined by a pickup coil.

## III. RESULTS

Figure 1 presents QOs from our SECUF, HFML-EMFL, and WNHMFC experiments, for rotations of the orientation of  $\mathbf{H}$  through the [001]-[100] rotation plane. Figure 1(e) collates the results of these experiments by plotting the oscillatory frequencies versus rotation angle, where the frequencies have been computed by

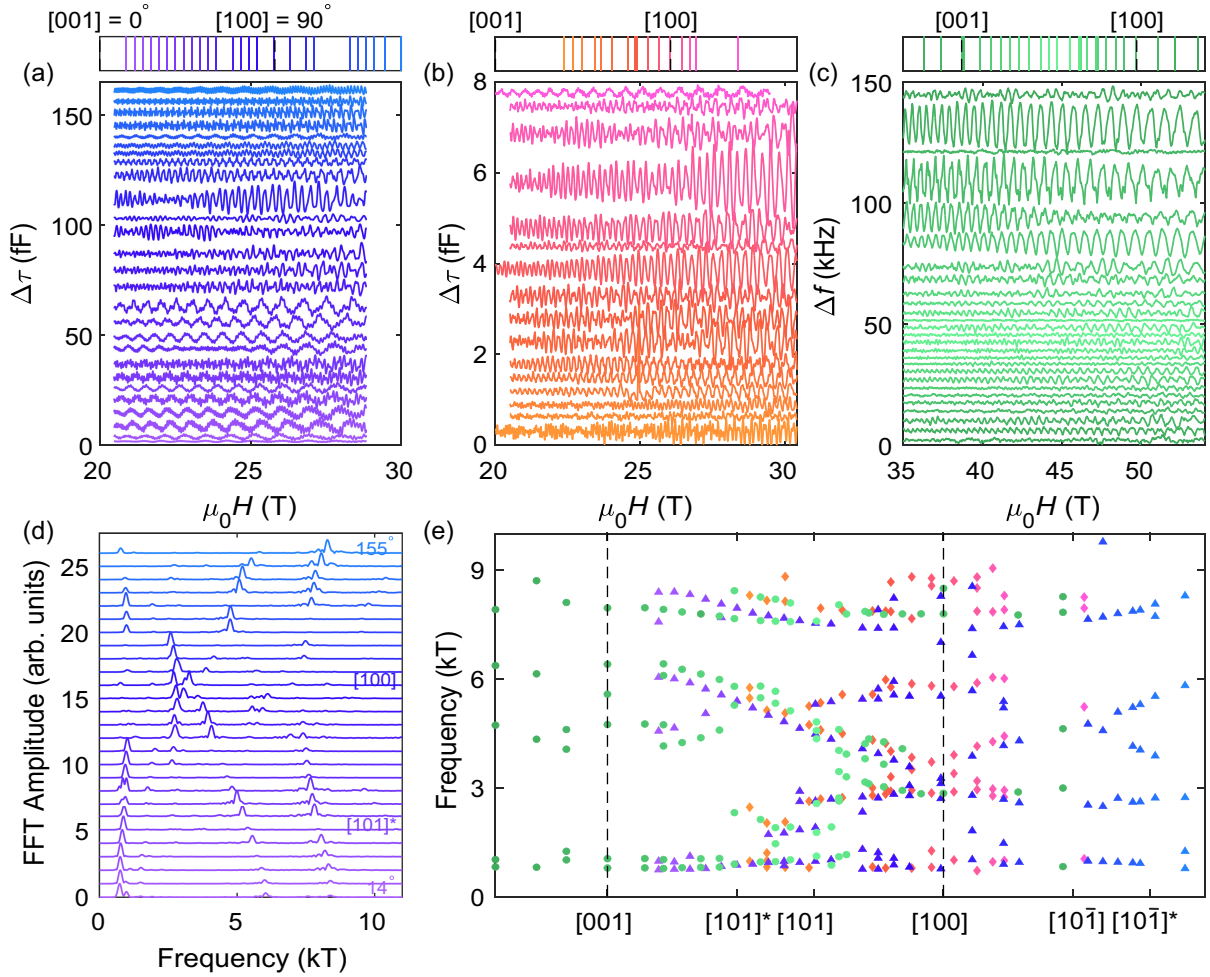


FIG. 1. Angle-dependent quantum oscillation measurements in RuO<sub>2</sub>. Background-subtracted magnetic torque ( $\Delta\tau$ ) measured at incremental angles in the [001]-[100] rotation plane recorded at (a) SECUF and (b) HFML-EMFL. (c) Quantum oscillations in the contactless resistivity measured at WNHMFC, also in the [001]-[100] plane. (d) Fast Fourier transforms (FFTs) of the data from (a) computed over 20.5–29.0 T. These spectra have been renormalized and offset for ease of presentation. (e) Angular distribution of quantum oscillatory frequency spectra, determined from performing FFTs for the data in (a)–(c), with symbols plotted in the same colors as the waveforms. Triangular points correspond to the SECUF measurements, diamond symbols refer to those performed at HFML-EMFL, while circular points refer to WNHMFC. Only fundamental components are included. Good correspondence is observed between the three measurements. Multiple frequency branches are resolved, indicating a complex multisheet fermiology.

fast Fourier transforms (FFTs) performed on the QO traces at each angle. Good correspondence between the three datasets is observed, with several frequency branches clearly resolved.

In Appendix A we examine the harmonic content of quantum oscillatory spectra. The pristine quality of single-crystal specimens measured in this study is underlined by the observation of an eighth harmonic component at low temperatures and high magnetic fields, at a frequency of 71.5 kT, indicating a mean free path  $\gtrsim 0.5 \mu\text{m}$ . This tallies with the residual resistivity of  $0.1 \mu\Omega\text{cm}$ , which by simple Drude considerations implies a mean free path of  $\approx 0.9 \mu\text{m}$ . In Appendix B we perform a Dingle

damping analysis of the electronic relaxation rate for different samples in different measurement systems, and find a similar level of sample quality for all specimens investigated in this study. Throughout the present section we focus solely on the fundamental QO frequency components.

In Fig. 2 we plot the evolution in temperature  $T$  of the oscillatory waveforms for torque measured with  $\mathbf{H}$  aligned along the [101] direction and close to the [101]\* direction, and for TDO with  $\mathbf{H} \parallel [101]^*$ . (See Appendix C for a discussion of the crystal orientation.) Numerous frequency components with a range of effective cyclotron masses are resolved. Good correspondence

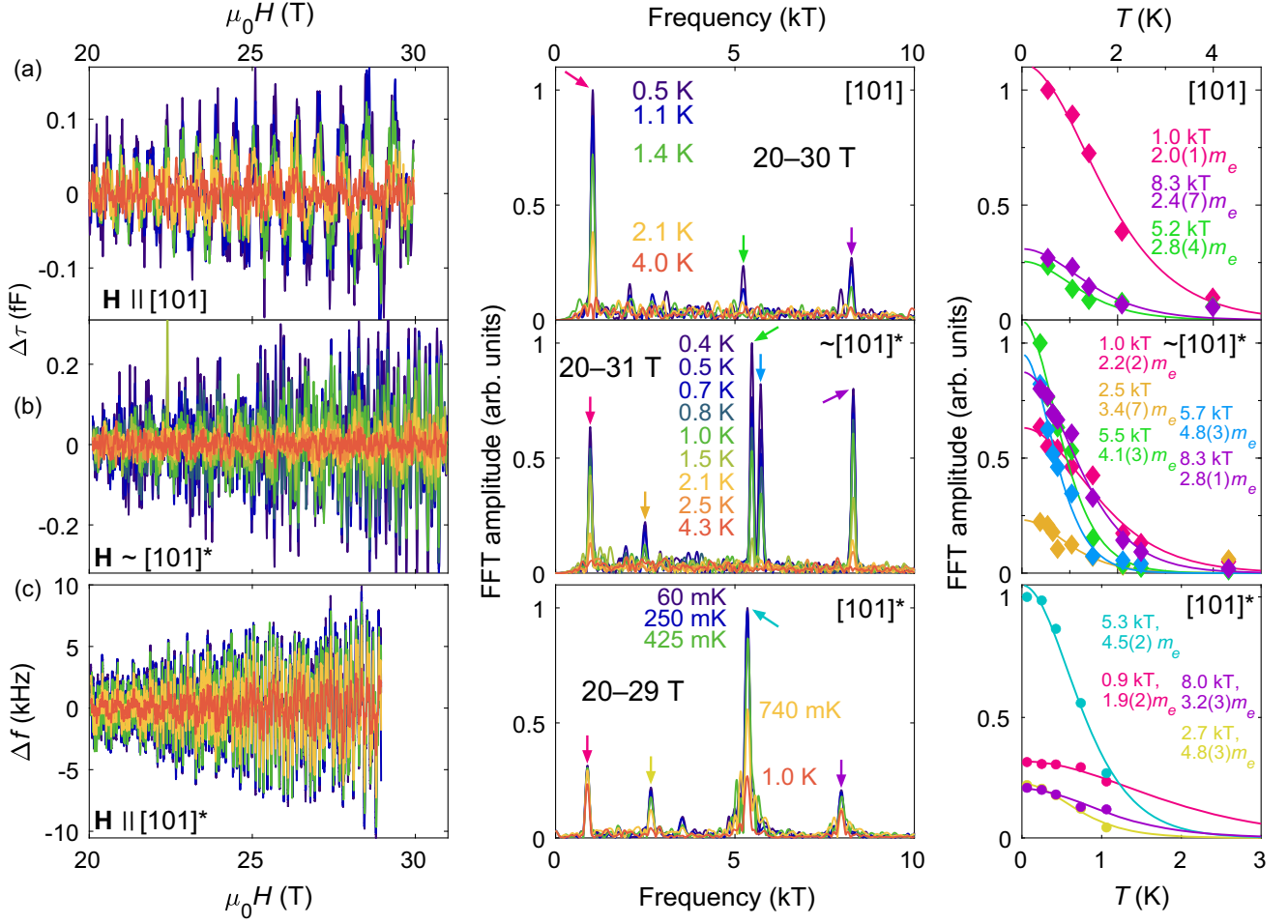


FIG. 2. Temperature evolution of (left) quantum oscillatory waveforms in  $\text{RuO}_2$ , (center) their corresponding FFT spectra, and (right) Lifshitz-Kosevich fits to the  $T$  dependence of FFT amplitudes for (a) torque measurements with  $\mathbf{H} \parallel [101]$ , (b) torque measurements with  $\mathbf{H}$  tilted  $3^\circ$  away from  $[101]^*$  toward  $[100]$ , and (c) TDO measurements with  $\mathbf{H} \parallel [101]^*$ . Multiple frequency branches are observed ranging from 900 T to 8.3 kT, with a spread of effective quasiparticle masses up to  $4.8(3)m_e$ .

is observed between the frequency spectra and effective masses resolved in both our magnetic torque and contactless resistivity experiments. As  $\tau$  is a bulk thermodynamic property of the material, this close correspondence indicates that our contactless resistivity measurements are sensitive to the bulk band structure of  $\text{RuO}_2$ .

In Fig. 3 we probe the Fermi surface by rotating  $\mathbf{H}$  between the  $[100]$  and  $[010]$  axes. Because of the tetragonal crystal symmetry, the frequency spectra should be degenerate for  $\mathbf{H} \parallel [100]$  and  $\parallel [010]$ . However, the frequency profile in Fig. 3(c) shows subtle differences between these two orientations. This is likely due to a slight misalignment of  $\sim 1^\circ$  causing a small but discernible spread of frequencies due to the presence of numerous extremal orbits about a complex Fermi surface structure.

Prior density functional theory (DFT) calculations [36] predicted that the observed QO frequencies should yield starkly different angular profiles depending on whether  $\text{RuO}_2$  is altermagnetic or paramagnetic. Figure 3 compares the angular dependence of QO frequencies observed by experiment with the DFT predictions for nonmagnetic and AM ordering reported in Ref. [36], along with the results of our own DFT calculations (see Appendix D for details). While the predicted AM Fermi surface from Ref. [36] would not be expected to yield any frequency components  $> 3$  kT in the  $[100]$ - $[010]$  rotation plane, the nonmagnetic Fermi surfaces from that study and from our calculations should both manifest a range of QO frequencies including a prominent branch at  $\approx 9$  kT. This prediction matches well with what we observe experimentally. Importantly, we also



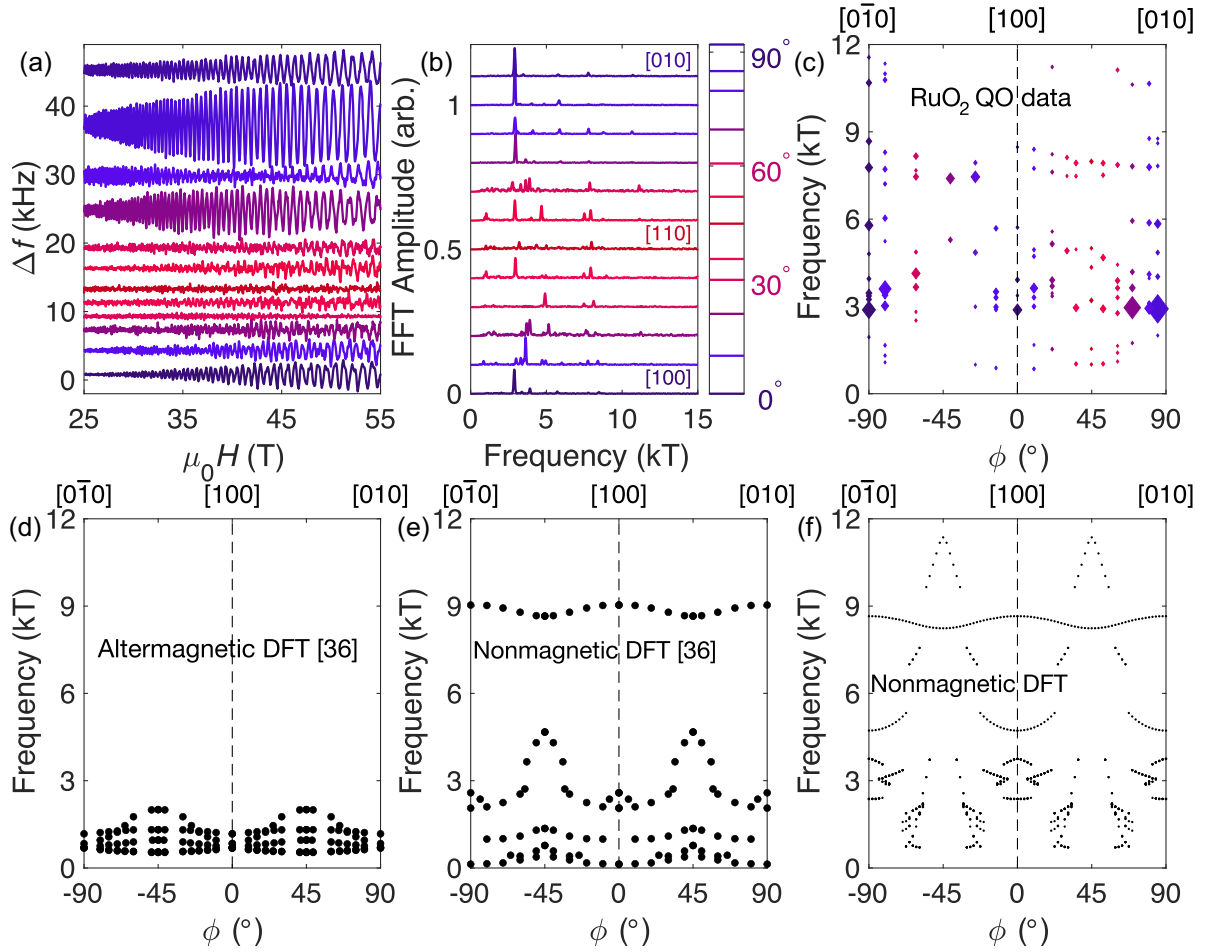


FIG. 3. Quantum oscillations in the [100]-[010] rotation plane. (a) SdH effect measurements of RuO<sub>2</sub> measured at WNHMFC with (b) the corresponding FFT spectra over the field range 25–55 T. (c) QO frequency versus rotation angle  $\phi$ , where  $\phi = 0^\circ$  corresponds to  $\mathbf{H} \parallel [100]$  while  $\phi = 90^\circ$  indicates  $\mathbf{H} \parallel [010]$ . The size of each point corresponds to the amplitude of that frequency component's FFT peak. A strong dependence of quantum oscillatory amplitude on magnetic field orientation is observed, indicative of considerable anisotropy in the curvature of the Fermi surface. (d) The predicted QO frequency versus angle profile for RuO<sub>2</sub> possessing AM ordering reported by Ref. [36] and (e) the expected profile in the absence of magnetic ordering. (f) The predicted angular QO frequency evolution from our DFT calculations for the nonmagnetic Fermi surface of RuO<sub>2</sub>. A complex structure of several frequency components is expected, similar to the experimental observation in (c).

resolve some high frequency components  $>10$  kT, which in Appendix E we show are a subtle feature expected for the scenario of the predicted paramagnetic Fermi surface of RuO<sub>2</sub>.

In Fig. 4 we collate the experimentally resolved QO frequency spectra in the [001]-[100] rotation plane from Fig. 1 and compare with the expectations from DFT calculations. Numerous features of the nonmagnetic Fermi

surface predictions match well with our experimental observations. These include a largely isotropic high frequency branch at around 8–9 kT, a low frequency branch around 1 kT, and a more complex intermediate branch that exhibits greater variation of frequency with angle than the other two branches. By contrast, the predicted AM angular frequency profile corresponds very poorly to our measurements.

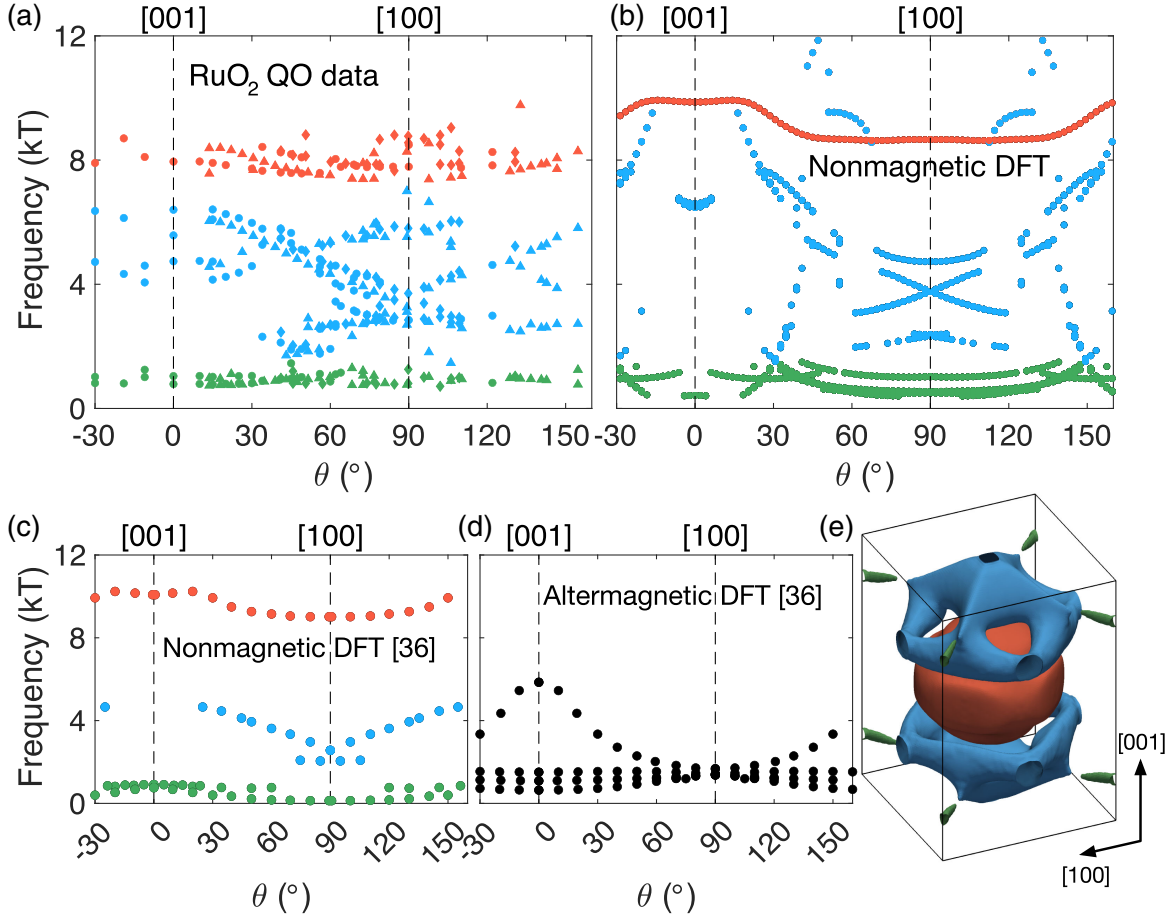


FIG. 4. Angular evolution of quantum oscillatory frequencies of RuO<sub>2</sub> in the [001]-[100] rotation plane. (a) Fundamental QO frequencies versus rotation angle  $\theta$  reproduced from Fig. 1. Here  $\theta = 0^\circ$  corresponds to  $\mathbf{H} \parallel [001]$  and  $\theta = 90^\circ$  to  $\mathbf{H} \parallel [100]$ . (b) Simulated QO frequencies versus  $\theta$  computed from our DFT calculations for a nonmagnetic Fermi surface. (c) The predicted angular frequency distribution in the absence of magnetism from Ref. [36] and (d) the alternative prediction for the case of AM ordering. (e) Rendering of the nonmagnetic RuO<sub>2</sub> Fermi surface from our DFT calculations. The red, blue, and green coloring throughout this figure is indicative of the three separate Fermi sheets.

#### IV. DISCUSSION

The presence of magnetic ordering in a material may introduce new periodic potentials and induce hybridization between localized and itinerant states, thereby opening energy gaps and shifting the electronic bands [37]. This typically leads to a significant reconstruction of the Fermi surface compared to the nonmagnetic scenario. The angular dependence of the quantum oscillatory frequency spectra that we observe in our experiments (Figs. 3 and 4) therefore sets strong constraints on the possible magnetic properties present within the bulk of RuO<sub>2</sub>.

If AM ordering were to be manifested throughout the bulk of RuO<sub>2</sub>, a markedly different Fermi surface geometry and topology has been expected [2,36] compared to the nonmagnetic case. In Appendix F we present our calculations for an AM Fermi surface. Interestingly, we found that upon initializing RuO<sub>2</sub> in a spin-polarized altermagnetic configuration, upon allowing the spins to relax the magnetic moments on the Ru ions substantially reduce. The resulting Fermi

surface subsequently relaxed toward that of the nonmagnetic scenario. Importantly, the DFT calculations of both the present study and Ref. [36] for the scenario of no magnetic ordering in RuO<sub>2</sub> capture the main features of the quantum oscillatory frequency spectra resolved by experiment.

Our QO data are well described by three Fermi surface sheets (Fig. 4). These include one large almost spherical pocket and a much smaller ellipsoid, the former yielding frequencies  $\approx 8$ – $9$  kT and the latter  $\approx 1$  kT (with 4 of these ellipsoids per Brillouin zone). The other Fermi surface sheet [colored blue in Fig. 4(e)] possesses a much more complex geometry, consisting of interconnected body and neck sections with numerous extremal orbital areas contributing to the observed QO frequency spectra. We note that this interpretation of three quite distinct Fermi sheets is broadly consistent with much earlier work on RuO<sub>2</sub> [38–42], in which this material was also considered to be nonmagnetic.

Recent photoemission experiments have discerned the presence of electronic states that appear to be confined to the surface of RuO<sub>2</sub> with low dispersion characteristic of low

Fermi velocities [24,25]. However, we do not resolve any signature of these states in either our dHvA or SdH measurements. That torque magnetometry is not sensitive to these surface states is unsurprising, since this technique probes a bulk thermodynamic property. Consider, for example, a cubic sample geometry—the ratio of surface to bulk unit cells in such a system is  $1 : 10^6$ ; therefore the contributory oscillatory amplitude from any surface component may be expected to be orders of magnitude smaller than that from the bulk [43]. By contrast, contactless resistivity measurements by the TDO and PDO techniques are much more sensitive to surface effects, as they operate at MHz frequencies for which the skin depth of a high conductivity metal such as RuO<sub>2</sub> is very short. However, the clearest photoemission spectra of the surface states appear to resolve a largely circular pocket that encloses an area (in reciprocal space) of  $\approx 1 \text{ \AA}^{-2}$  [24,25], which for  $\mathbf{H} \parallel [110]^*$  would yield QOs with a frequency  $\approx 10 \text{ kT}$ . At  $\mu_0 H = 30 \text{ T}$ , the corresponding cyclotron orbit of such a pocket would possess a diameter (in real space) of  $\approx 200 \text{ nm}$ , necessitating a long mean free path in the surface layer. While the bulk of our samples indeed possesses such a long mean free path (see Appendix A), if the surface states are topological as has been proposed [25], then they will be confined to a very small volumetric fraction of the sample right at the surface. It would be reasonable to assume that the mean free path at the surface is less than in the bulk, which would in turn explain why we did not appear to resolve any signature of these surface states. Furthermore, let us consider the skin depth  $\delta$  probed by a contactless conductivity measurement of a material with magnetic susceptibility  $\chi$  and resistivity  $\rho$ , which may be written as  $\delta = \sqrt{(2\rho)/(\omega\mu)}$ , where  $\omega$  is the excitation frequency and  $\mu = \mu_0(1 + \chi)$  [44]. For our TDO experiments presented in Fig. 2(c) the TDO circuit rang at  $110 \text{ MHz}$ . Given the residual resistivity of  $0.1 \text{ }\mu\Omega\text{cm}$  this yields  $\delta = 1.1 \text{ }\mu\text{m}$ . Therefore,  $\delta$  extends approximately 2000 unit cells in the direction normal to the surface. From this analysis it is difficult to quantitatively estimate the depth to which these surface states are present in RuO<sub>2</sub>; however, these findings suggest they are localized to a small volume very close to the surface layer. Additionally, we note that some of the surface sheets appear to be quasi-1D, which in a magnetic field would yield open orbits that do not produce QOs.

The pronounced disagreement between the expected geometry of the AM Fermi surface of RuO<sub>2</sub> and our experimental observations corroborates the growing body of evidence in favor of RuO<sub>2</sub> not being magnetically ordered [21,22,24,25,45,46]. Reconciling a nonmagnetic ground state with phenomena including the anomalous Hall effect, spin-current generation, and magnetic circular dichroism [15–20] therefore presents an outstanding challenge. The anomalous character of the electronic surface states resolved by photoemission spectroscopy—reported to display a Rashba-like spin splitting [24] with nontrivial topology [25]—may be the cause of several of these observations. It has also been proposed that RuO<sub>2</sub> thin films may exhibit a different magnetic

character compared to single crystals [47], and that the bulk magnetic properties may be acutely sensitive to the density of ruthenium vacancies [48]. We note that the observation of very high frequency QO components, with multiple harmonics up to  $71.5 \text{ kT}$ , implies a long mean free path and thus a very low density of vacancies in our measured crystals.

In conclusion, we performed a quantum oscillation study of the metallic altermagnet candidate RuO<sub>2</sub>. We resolved a Fermi surface geometry that matches well with the predicted electronic structure in the absence of magnetism; whereas, the expected angular dependence of quantum oscillatory frequency spectra for the case of altermagnetic ordering disagrees markedly with our experimental observations. Our findings strongly support the scenario that the magnetic ground state of RuO<sub>2</sub> is paramagnetic in character.

## ACKNOWLEDGMENTS

We gratefully acknowledge stimulating discussions with A. Agarwal, D. Calugaru, D. Chichinadze, A. Coldea, B. Ramshaw, T. Sato, D. Shaffer, R.-J. Slager, and S. Souma. This project was supported by the EPSRC of the UK (Grant No. EP/X011992/1). We acknowledge the support of HFML-RU/NWO-I, member of the European Magnetic Field Laboratory (EMFL) and the Engineering and Physical Sciences Research Council (EPSRC, UK) via its membership to the EMFL (Grant No. EP/N01085X/1). A portion of this work was carried out at the Synergetic Extreme Condition User Facility (SECUF) [49]. This work was supported by JSPS KAKENHI Grants No. JP22H01168 and No. JP23K22439. A portion of this work was performed at the National High Magnetic Field Laboratory, which is supported by National Science Foundation Cooperative Agreement No. DMR-2128556 and the State of Florida. Computational work in this study was performed using the ARCHER2 UK National Supercomputing Service [50] and resources provided by the Cambridge Service for Data Driven Discovery (CSD3) operated by the University of Cambridge Research Computing Service, provided by Dell EMC and Intel using Tier-2 funding from EPSRC (Capital Grant No. EP/T022159/1), and DiRAC funding from the Science and Technology Facilities Council. S. P. and Y. M. acknowledge support of the JST Sakura Science Program. H. M. acknowledges support from the Kyoto University Foundation. T. I. W. and A. G. E. acknowledge support from QuantEmX grants from ICAM and the Gordon and Betty Moore Foundation through Grant No. GBMF9616 and from the U.S. National Science Foundation (NSF) Grant No. 2201516 under the Accelnet program of Office of International Science and Engineering (OISE). A. G. E. acknowledges support from Sidney Sussex College (University of Cambridge).

## DATA AVAILABILITY

The datasets that support the findings of this study are openly available from the University of Cambridge Apollo Repository [51].

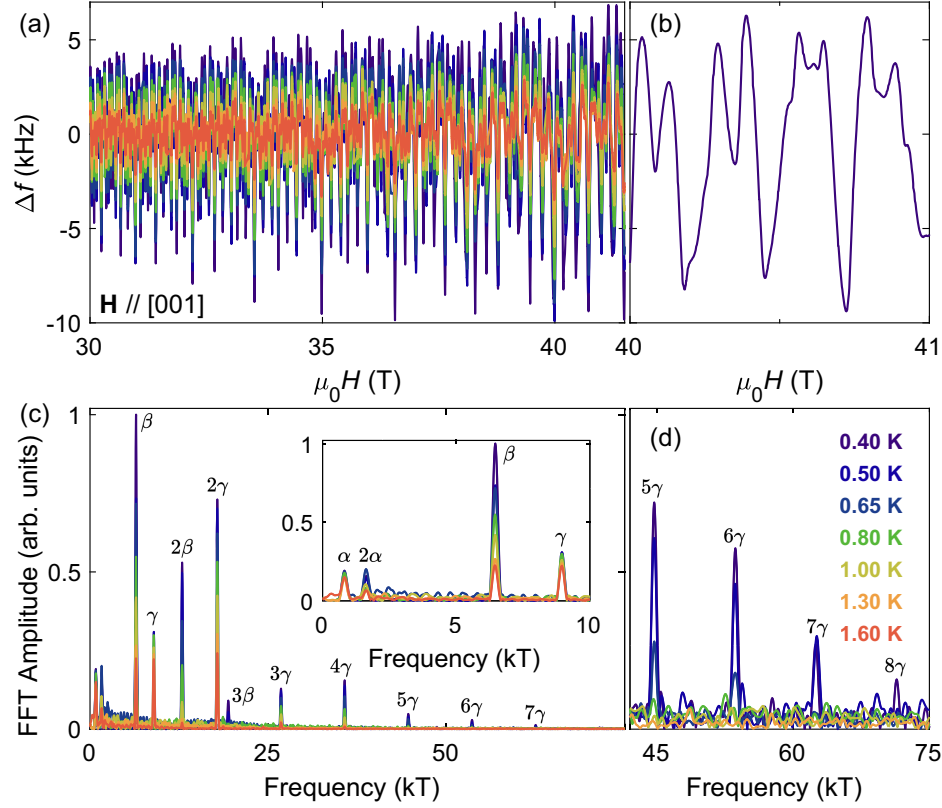


FIG. 5. High harmonic frequency components. (a) QOs in the contactless resistivity of RuO<sub>2</sub> measured by the TDO technique at NHMFL. (b) Enlargement between 40 and 41 T of the base temperature sweep in (a), with several fast frequency components visible. (c) FFT of the data in (a) over the field interval 30–41.5 T, with numerous harmonics identified. The inset shows the 0–10 kT frequency range, in which the three fundamental frequencies  $\alpha$ ,  $\beta$ , and  $\gamma$  are labeled. (d) Enlargement of the highest frequency Fourier spectra, in which the eighth harmonic of the  $\gamma$  branch is resolvable at low  $T$ .

## APPENDIX A: HARMONIC CONTENT OF QUANTUM OSCILLATORY FREQUENCY SPECTRA

In Fig. 5 we present contactless conductivity data for an RuO<sub>2</sub> single crystal measured by the TDO method at NHMFL in high magnetic field strengths up to 41.5 T, with the field oriented along the [001] direction. Numerous harmonic components are visible in the Fourier spectra, which are tabulated in Table I.

A QO frequency  $f$  is related to an extremal Fermi surface cross-sectional area (in reciprocal space) [52]. This area corresponds to a quasiparticle orbit, in real space, which for a simple circular geometry would possess a radius  $r = \sqrt{2\hbar f / e(\mu_0 H)^2}$ , where  $e$  is the elementary charge and  $\hbar$  the reduced Planck constant [26]. Samples with long mean free paths  $\lambda$  are therefore required in order to resolve high frequency contributions, as QOs of frequency  $f$  will only be manifested if  $2r \lesssim \lambda$ . Access to high magnetic fields is valuable, as increasing  $H$  reduces  $r$ . The observation of the eighth harmonic of the  $\gamma$  branch, with  $f = 71.5$  T resolved for  $\mu_0 H \gtrsim 36$  T, therefore indicates a long mean free path of  $\lambda \gtrsim 0.5$   $\mu\text{m}$ .

TABLE I. List of harmonic components and their corresponding frequencies and effective masses from the data presented in Fig. 5 for  $\mathbf{H} \parallel [001]$ . Effective masses are quoted only for branches with sufficient amplitude to be well resolved at elevated temperatures. The  $n$ th harmonic is easily identifiable as possessing  $n$  times the frequency and mass of the corresponding fundamental orbit [26].

Harmonic index	Frequency (kT)	Effective mass ( $m_e$ )
$\alpha$	0.82	2.3(3)
$2\alpha$	1.63	5(1)
$\beta$	6.46	6.6(5)
$2\beta$	12.9	11(1)
$3\beta$	19.4	...
$\gamma$	8.95	2.5(2)
$2\gamma$	17.9	5.3(1)
$3\gamma$	26.8	7.8(3)
$4\gamma$	35.7	9.8(3)
$5\gamma$	44.7	12(1)
$6\gamma$	53.6	13(2)
$7\gamma$	62.6	...
$8\gamma$	71.5	...



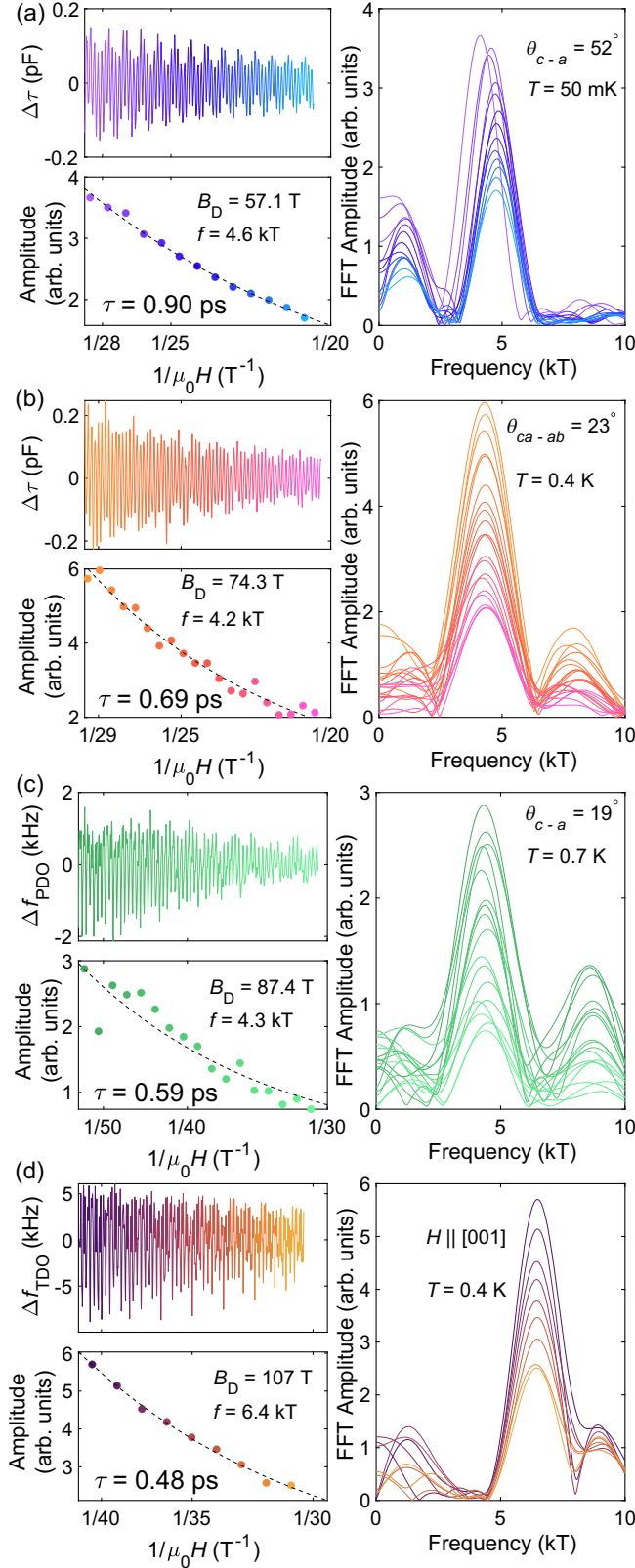


FIG. 6. Dingle factor  $B_D$  extracted from the dependence of quantum oscillatory amplitude on magnetic field strength for the four sets of measurements presented in this study. Individual panels correspond to the measurements performed at (a) SECUF, (b) HFML-EMFL, (c) WHMFC, and (d) NHMFL.

## APPENDIX B: DINGLE DAMPING ANALYSIS OF THE ELECTRONIC RELAXATION TIME

Here we present a Dingle damping analysis [53] of quantum oscillatory waveforms measured on four separate samples at four different high magnetic field facilities, to determine the relaxation time  $\tau$ . The Dingle damping factor  $R_D$  may be described as

$$R_D = \exp \left[ \frac{-\pi m_b}{e\tau\mu_0 H} \right], \quad (\text{B1})$$

where  $e$  is the elementary charge,  $H$  the applied field, and  $m_b$  the band mass, which we take to be 3 times the electron rest mass. The Dingle factor,  $B_D = \pi m_b / e\tau$ , is noted for each dataset in Fig. 6. We sliced the data into equal regions of inverse field ( $1/\mu_0 H$ ) length and computed the FFT for each section. The oscillation amplitude was then taken as the height of the FFT peak for each slice. Because of incoherent scattering the oscillatory amplitude grows as the field increases (or, equivalently, as inverse field decreases), as the cyclotron radius shrinks as field grows. By fitting the dependence of a given frequency component's amplitude to magnetic field strength using Eq. (B1), we extract the relaxation time for each sample, stated in Fig. 6. We find only a small variation in relaxation times (within a factor of 2) between the samples, indicating that they all possess a similarly high level of crystalline quality.

## APPENDIX C: CRYSTALLOGRAPHIC ORIENTATION

The tetragonal, rutile crystal structure of RuO<sub>2</sub> is depicted in Fig. 7. In Figs. 1 and 2 we refer to  $\mathbf{H}$  oriented along the  $[101]^*$  orientation. This asterisk notation denotes the  $ac$  diagonal in reciprocal space, which is the same

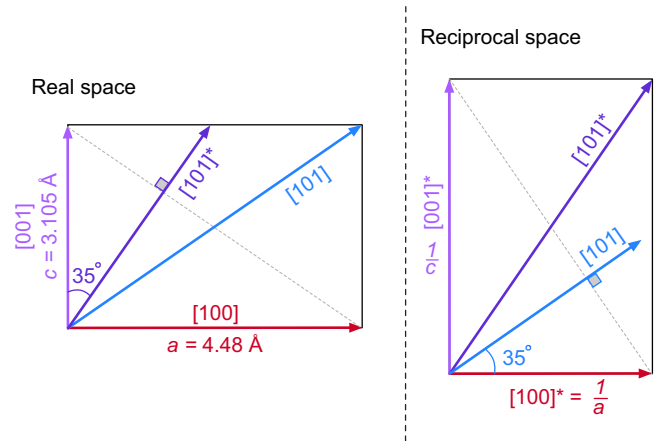


FIG. 7. 2D representation of the crystal structure of RuO<sub>2</sub>, with a diagrammatic illustration of the  $[101]$  and  $[101]^*$  directions that are separated by 20° in the  $c$ - $a$  plane. In real space, the  $[101]^*$  direction is normal to the  $(101)$  surface.

direction as the vector normal to the (101) surface in real space [54].

#### APPENDIX D: DENSITY FUNCTIONAL THEORY CALCULATIONS

DFT calculations for RuO<sub>2</sub> were performed within the full electron, linearized augmented plane-wave package WIEN2K [55]. The electronic structure was converged on an  $11 \times 11 \times 16$  Monkhorst-Pack  $k$  mesh within the Brillouin zone of the primitive unit cell using the generalized gradient approximation exchange-correlation potential. The effects of spin-orbit coupling were considered where the easy axis was assumed to be along the [001] direction. Relativistic local orbital (RLO) states were added to the basis for Ru to improve the modeling of its  $p$ -semicore states. No RLOs were added for O.

We assumed that P4/*mmn* RuO<sub>2</sub> adopts lattice parameters 4.50, 4.50, 3.10 Å. Within the unit cell there are two equivalent Ru sites,

Atom	$X$	$Y$	$Z$
Ru <sub>1</sub>	0.00	0.00	0.00
Ru <sub>2</sub>	0.50	0.50	0.50

and four equivalent oxygen sites,

Atom	$X$	$Y$	$Z$
O <sub>1</sub>	0.31	0.31	0.00
O <sub>2</sub>	0.69	0.69	0.00
O <sub>3</sub>	0.19	0.19	0.50
O <sub>4</sub>	0.81	0.81	0.50

We performed a single non-self-consistent DFT iteration of our converged electronic structure, projected onto a  $19 \times 19 \times 27$  Monkhorst-Pack  $k$  mesh, with which we performed our analysis of the expected quantum oscillation frequencies corresponding to the calculated Fermi surface. The angular evolution of quantum oscillatory frequencies was determined using SKEAF [56]; Fermi surface visualization was performed using py\_FS [57].

#### APPENDIX E: HIGH FREQUENCY OSCILLATION IN [100]-[010] ROTATION PLANE

A key difference between the expected Fermi surface geometries for the different scenarios of altermagnetism and paramagnetism in RuO<sub>2</sub> is the predicted presence of large Fermi sheets in the nonmagnetic case, which would exhibit high QO frequencies. At a tilt angle of 61° from [100] toward [010] we observed a frequency component at 11.12 kT (Fig. 8). Analysis of the lower frequency components finds that this high frequency is not a harmonic of a lower frequency branch, nor is it the result of a summation of two of the lower components. Instead, it

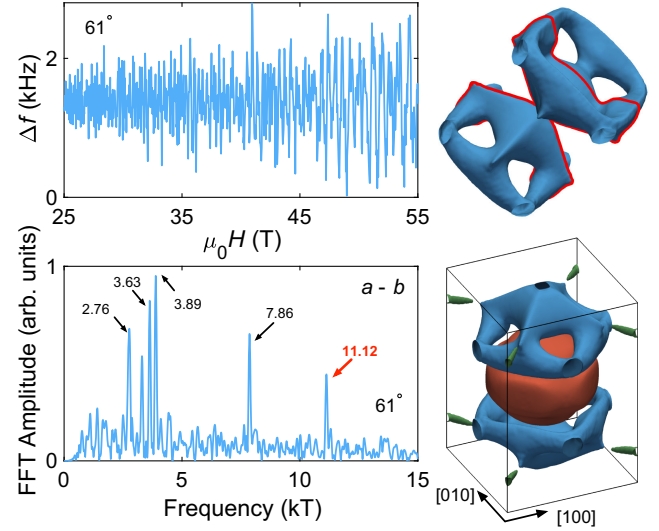


FIG. 8. Identification of a large area QO orbit. Quantum oscillatory waveform and corresponding FFT spectra for  $\mathbf{H}$  tilted 61° from [100] toward [010]. The peak indicated with the red arrow, at a frequency of 11.12 kT, does not correspond to a multiplication or summation of the lower frequency peaks. Therefore, it appears to represent a fundamental frequency component. This corresponds well to the expectation from our DFT calculations of an orbit of large area occurring for a small range of angles close to the [110] direction, where one of the Fermi sheets (namely, that colored in blue here and in Fig. 4) possesses a closed orbit that traverses the first two Brillouin zones (traced in red in upper right Fermi surface visualization). This observation lends strong confidence to our identification of a nonmagnetic Fermi surface in RuO<sub>2</sub>.

appears to correspond to a large orbit spanning the first two Brillouin zones, only manifested for intermediate angles for  $\mathbf{H}$  applied near the center of the  $a$ - $b$  rotation plane [which in Fig. 3(f) is predicted to form a spread of frequencies between 9 and 12 kT]. The observation of this frequency component therefore argues strongly in favor of the nonmagnetic Fermi surface scenario we calculate for RuO<sub>2</sub>.

#### APPENDIX F: DISCUSSION OF THE ALTERMAGNETIC FERM SURFACE SCENARIO FOR RuO<sub>2</sub>

We performed calculations of the electronic structure of RuO<sub>2</sub> based on a number of other starting electronic configurations to complement our nonmagnetic Fermi surface calculations. Interestingly, we found that if RuO<sub>2</sub> is initialized in a spin-polarized altermagnetic configuration, when the spins relax, the magnetic moments on the Ru ions substantially reduce, with the resulting Fermi surface relaxing toward that of the nonmagnetic scenario. To achieve a spin-split Fermi surface within WIEN2K, we had to apply a staggered magnetic moment to the atomic spheres of the Ru ions. We were able to force the system to converge to a spin-split electronic structure with sizable

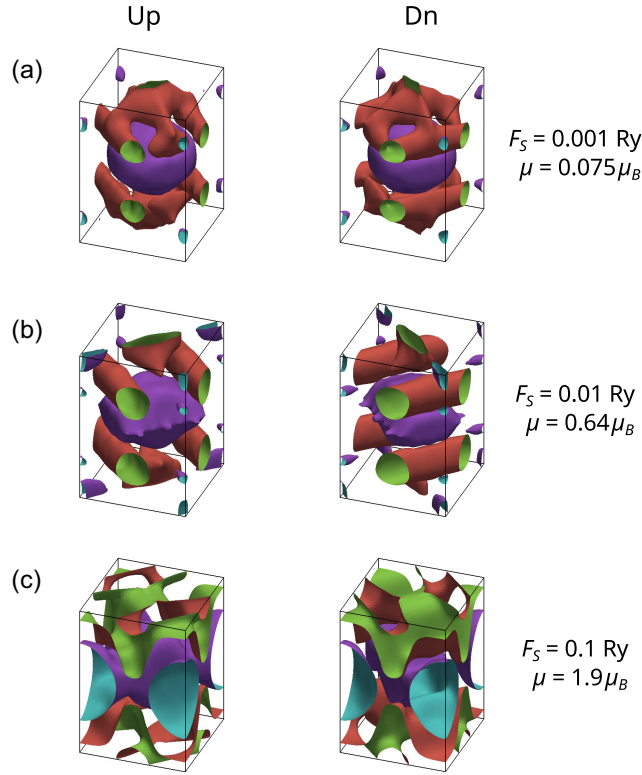


FIG. 9. Fermi surfaces of RuO<sub>2</sub> from DFT calculations where a staggered field has been applied to the atomic spheres of Ru to induce spin splitting. Dn denotes the spin-down Fermi sheets. (a) A small staggered field  $F_s$  of 0.001 Ry slightly deforms the Fermi surface of RuO<sub>2</sub>, inducing some spin splitting. The associated moment on the Ru ions of this electronic structure is  $0.075\mu_B$ , which is already larger than the experimentally determined limit reported by Refs. [21,22]. Increasing the staggered field (b),(c) induces a more pronounced splitting of the surfaces, resulting in semiellipsoidal surfaces when the staggered field is 0.1 Ry. The moment associated with Ru ions here is  $1.9\mu_B$ , which is unphysically large.

moments on the Ru ions by applying a staggered field in opposing directions to the atomic spheres of Ru. In Fig. 9, we show how applying increasingly large staggered fields allows us to almost continuously deform the Fermi surface from the nonmagnetic geometry to an electronic structure that resembles that predicted in Ref. [36]. The double-ellipsoid type altermagnetic Fermi surface of Ref. [36] required a substantial staggered field of  $\pm 0.1$  Ry, inducing a  $1.9\mu_B$  moment on the Ru ions, substantially larger than the upper limit placed on the moment by recent experimental measurements [21,22].

[1] L. Šmejkal, J. Sinova, and T. Jungwirth, *Beyond conventional ferromagnetism and antiferromagnetism: A phase with nonrelativistic spin and crystal rotation symmetry*, *Phys. Rev. X* **12**, 031042 (2022).

[2] L. Šmejkal, J. Sinova, and T. Jungwirth, *Emerging research landscape of altermagnetism*, *Phys. Rev. X* **12**, 040501 (2022).

[3] K.-H. Ahn, A. Hariki, K.-W. Lee, and J. Kuneš, *Antiferromagnetism in RuO<sub>2</sub> as d-wave Pomeranchuk instability*, *Phys. Rev. B* **99**, 184432 (2019).

[4] M. Naka, S. Hayami, H. Kusunose, Y. Yanagi, Y. Motome, and H. Seo, *Spin current generation in organic antiferromagnets*, *Nat. Commun.* **10**, 4305 (2019).

[5] Z. Savitsky, *Researchers discover new kind of magnetism*, *Science* **383**, 574 (2024).

[6] S. Hayami, Y. Yanagi, and H. Kusunose, *Momentum-dependent spin splitting by collinear antiferromagnetic ordering*, *J. Phys. Soc. Jpn.* **88**, 123702 (2019).

[7] I. Mazin and The PRX Editors, *Editorial: Altermagnetism—A new punch line of fundamental magnetism*, *Phys. Rev. X* **12**, 040002 (2022).

[8] L. Šmejkal, R. González-Hernández, T. Jungwirth, and J. Sinova, *Crystal time-reversal symmetry breaking and spontaneous Hall effect in collinear antiferromagnets*, *Sci. Adv.* **6**, eaaz8809 (2020).

[9] S. S. Fender, O. Gonzalez, and D. K. Bediako, *Altermagnetism: A chemical perspective*, *J. Am. Chem. Soc.* **147**, 2257 (2025).

[10] C. Song, H. Bai, Z. Zhou, L. Han, H. Reichlova, J. H. Dil, J. Liu, X. Chen, and F. Pan, *Altermagnets as a new class of functional materials*, *Nat. Rev. Mater.* **10**, 473 (2025).

[11] L. Bai, W. Feng, S. Liu, L. Šmejkal, Y. Mokrousov, and Y. Yao, *Altermagnetism: Exploring new frontiers in magnetism and spintronics*, *Adv. Funct. Mater.* **34**, 2409327 (2024).

[12] P. Khalili Amiri, C. Phatak, and G. Finocchio, *Prospects for antiferromagnetic spintronic devices*, *Annu. Rev. Mater. Res.* **54**, 117 (2024).

[13] T. Berlijn, P. C. Snijders, O. Delaire, H.-D. Zhou, T. A. Maier, H.-B. Cao, S.-X. Chi, M. Matsuda, Y. Wang, M. R. Koehler, P. R. C. Kent, and H. H. Weitering, *Itinerant antiferromagnetism in RuO<sub>2</sub>*, *Phys. Rev. Lett.* **118**, 077201 (2017).

[14] Z. H. Zhu, J. Stremper, R. R. Rao, C. A. Occhialini, J. Pellicciari, Y. Choi, T. Kawaguchi, H. You, J. F. Mitchell, Y. Shao-Horn, and R. Comin, *Anomalous antiferromagnetism in metallic RuO<sub>2</sub> determined by resonant x-ray scattering*, *Phys. Rev. Lett.* **122**, 017202 (2019).

[15] Z. Feng, X. Zhou, L. Šmejkal, L. Wu, Z. Zhu, H. Guo, R. González-Hernández, X. Wang, H. Yan, P. Qin *et al.*, *An anomalous Hall effect in altermagnetic ruthenium dioxide*, *Nat. Electron.* **5**, 735 (2022).

[16] A. Bose, N. J. Schreiber, R. Jain, D.-F. Shao, H. P. Nair, J. Sun, X. S. Zhang, D. A. Muller, E. Y. Tsybal, D. G. Schlom *et al.*, *Tilted spin current generated by the collinear antiferromagnet ruthenium dioxide*, *Nat. Electron.* **5**, 267 (2022).

[17] H. Bai, L. Han, X. Y. Feng, Y. J. Zhou, R. X. Su, Q. Wang, L. Y. Liao, W. X. Zhu, X. Z. Chen, F. Pan, X. L. Fan, and C. Song, *Observation of spin splitting torque in a collinear antiferromagnet RuO<sub>2</sub>*, *Phys. Rev. Lett.* **128**, 197202 (2022).

[18] S. Karube, T. Tanaka, D. Sugawara, N. Kadoguchi, M. Kohda, and J. Nitta, *Observation of spin-splitter torque in collinear antiferromagnetic RuO<sub>2</sub>*, *Phys. Rev. Lett.* **129**, 137201 (2022).



- [19] Y. Guo, J. Zhang, Z. Zhu, Y.-y. Jiang, L. Jiang, C. Wu, J. Dong, X. Xu, W. He, B. He *et al.*, *Direct and inverse spin splitting effects in altermagnetic RuO<sub>2</sub>*, *Adv. Sci.* **11**, 2400967 (2024).
- [20] O. Fedchenko, J. Minár, A. Akashdeep, S. W. D'Souza, D. Vasilyev, O. Tkach, L. Odenbreit, Q. Nguyen, D. Kutnyakhov, N. Wind *et al.*, *Observation of time-reversal symmetry breaking in the band structure of altermagnetic RuO<sub>2</sub>*, *Sci. Adv.* **10**, eadj4883 (2024).
- [21] M. Hiraishi, H. Okabe, A. Koda, R. Kadono, T. Muroi, D. Hirai, and Z. Hiroi, *Nonmagnetic ground state in RuO<sub>2</sub> revealed by muon spin rotation*, *Phys. Rev. Lett.* **132**, 166702 (2024).
- [22] P. Keßler, L. Garcia-Gassull, A. Suter, T. Prokscha, Z. Salman, D. Khalyavin, P. Manuel, F. Orlandi, I. I. Mazin, R. Valentí, and S. Moser, *Absence of magnetic order in RuO<sub>2</sub>: Insights from  $\mu$ SR spectroscopy and neutron diffraction*, *npj Spintronics* **2**, 50 (2024).
- [23] Z. Lin, D. Chen, W. Lu, X. Liang, S. Feng, K. Yamagami, J. Osiecki, M. Leandersson, B. Thiagarajan, J. Liu, C. Felser, and J. Ma, *Observation of giant spin splitting and d-wave spin texture in room temperature altermagnet RuO<sub>2</sub>*, *arXiv:2402.04995*.
- [24] J. Liu *et al.*, *Absence of altermagnetic spin splitting character in rutile oxide RuO<sub>2</sub>*, *Phys. Rev. Lett.* **133**, 176401 (2024).
- [25] T. Osumi, K. Yamauchi, S. Souma, P. Shubhankar, A. Honma, K. Nakayama, K. Ozawa, M. Kitamura, K. Horiba, H. Kumigashira, C. Bigi, F. Bertran, T. Oguchi, T. Takahashi, Y. Maeno, and T. Sato, *Spin-degenerate bulk bands and topological surface states of RuO<sub>2</sub>*, *arXiv:2501.10649*.
- [26] D. Shoenberg, *Magnetic Oscillations in Metals* (Cambridge University Press, Cambridge, England, 1984).
- [27] Z.-X. Li, H. Zhou, X. Wan, and W. Chen, *Diagnosing altermagnetic phases through quantum oscillations*, *Phys. Rev. B* **111**, 125119 (2025).
- [28] S. Paul, G. Mattoni, H. Matsuki, T. Johnson, C. Sow, S. Yonezawa, and Y. Maeno, *Growth of ultra-clean single crystals of RuO<sub>2</sub>*, *arXiv:2505.07201*.
- [29] C. T. Van Degrift, *Tunnel diode oscillator for 0.001 ppm measurements at low temperatures*, *Rev. Sci. Instrum.* **46**, 599 (1975).
- [30] M. M. Altarawneh, C. H. Mielke, and J. S. Brooks, *Proximity detector circuits: An alternative to tunnel diode oscillators for contactless measurements in pulsed magnetic field environments*, *Rev. Sci. Instrum.* **80**, 066104 (2009).
- [31] C. Bergemann, S. Julian, A. P. Mackenzie, A. Tyler, D. Farrell, Y. Maeno, and S. Nishizaki, *Quantum oscillations and overcritical torque interaction in Sr<sub>2</sub>RuO<sub>4</sub>*, *Physica (Amsterdam)* **317C–318C**, 444 (1999).
- [32] S. E. Sebastian, N. Harrison, E. Palm, T. Murphy, C. Mielke, R. Liang, D. Bonn, W. Hardy, and G. Lonzarich, *A multi-component Fermi surface in the vortex state of an underdoped high-T<sub>c</sub> superconductor*, *Nature (London)* **454**, 200 (2008).
- [33] N. Matsuyama, T. Nomura, S. Imajo, T. Nomoto, R. Arita, K. Sudo, M. Kimata, N. D. Khanh, R. Takagi, Y. Tokura, S. Seki, K. Kindo, and Y. Kohama, *Quantum oscillations in the centrosymmetric skyrmion-hosting magnet GdRu<sub>2</sub>Si<sub>2</sub>*, *Phys. Rev. B* **107**, 104421 (2023).
- [34] A. G. Eaton, T. I. Weinberger, N. J. M. Popiel, Z. Wu, A. J. Hickey, A. Cabala, J. Pospíšil, J. Prokleška, T. Haidamak, G. Bastien, P. Opletal, H. Sakai, Y. Haga, R. Nowell, S. M. Benjamin, V. Sechovský, G. G. Lonzarich, F. M. Grosche, and M. Vališka, *Quasi-2D Fermi surface in the anomalous superconductor UTe<sub>2</sub>*, *Nat. Commun.* **15**, 223 (2024).
- [35] T. I. Weinberger, Z. Wu, D. E. Graf, Y. Skourski, A. Cabala, J. Pospíšil, J. Prokleška, T. Haidamak, G. Bastien, V. Sechovský, G. G. Lonzarich, M. Vališka, F. M. Grosche, and A. G. Eaton, *Quantum interference between quasi-2D Fermi surface sheets in UTe<sub>2</sub>*, *Phys. Rev. Lett.* **132**, 266503 (2024).
- [36] Y. Huang, J. Lai, J. Zhan, T. Yu, R. Chen, P. Liu, X.-Q. Chen, and Y. Sun, *Ab initio study of quantum oscillations in altermagnetic and nonmagnetic phases of RuO<sub>2</sub>*, *Phys. Rev. B* **110**, 144410 (2024).
- [37] R. E. Peierls, *Quantum Theory of Solids* (Clarendon Press, Oxford, 1955).
- [38] S. Marcus and S. Butler, *Measurement of the de Haas–van Alphen effect in the rutile structure RuO<sub>2</sub>*, *Phys. Lett. A* **26**, 518 (1968).
- [39] R. Slivka and D. Langenberg, *Azbel'–Kaner cyclotron resonance in ruthenium dioxide*, *Phys. Lett.* **28A**, 169 (1968).
- [40] J. E. Graebner, E. S. Greiner, and W. D. Ryden, *Magneto-thermal oscillations in RuO<sub>2</sub>, OsO<sub>2</sub>, and IrO<sub>2</sub>*, *Phys. Rev. B* **13**, 2426 (1976).
- [41] L. F. Mattheiss, *Electronic structure of RuO<sub>2</sub>, OsO<sub>2</sub>, and IrO<sub>2</sub>*, *Phys. Rev. B* **13**, 2433 (1976).
- [42] B. Y. Yavorsky, O. Krasovska, E. Krasovskii, A. Yaresko, and V. Antonov, *Ab initio calculation of the Fermi surface of RuO<sub>2</sub>*, *Physica (Amsterdam)* **225B**, 243 (1996).
- [43] M. Hartstein, W. Toews, Y.-T. Hsu, B. Zeng, X. Chen, M. C. Hatnean, Q. Zhang, S. Nakamura, A. Padgett, G. Rodway-Gant *et al.*, *Fermi surface in the absence of a Fermi liquid in the Kondo insulator SmB<sub>6</sub>*, *Nat. Phys.* **14**, 166 (2018).
- [44] Z. Wu, T. I. Weinberger, J. Chen, A. Cabala, D. V. Chichinadze, D. Shaffer, J. Pospíšil, J. Prokleška, T. Haidamak, G. Bastien, V. Sechovský, A. J. Hickey, M. J. Mancera-Ugarte, S. Benjamin, D. E. Graf, Y. Skourski, G. G. Lonzarich, M. Vališka, F. M. Grosche, and A. G. Eaton, *Enhanced triplet superconductivity in next-generation ultraclean UTe<sub>2</sub>*, *Proc. Natl. Acad. Sci. U.S.A.* **121**, e2403067121 (2024).
- [45] M. Wenzel, E. Uykur, S. Rößler, M. Schmidt, O. Janson, A. Tiwari, M. Dressel, and A. A. Tsirlin, *Fermi-liquid behavior of nonaltermagnetic RuO<sub>2</sub>*, *Phys. Rev. B* **111**, L041115 (2025).
- [46] L. Kiefer, F. Wirth, A. Bertin, P. Becker, L. Bohatý, K. Schmalzl, A. Stunault, J. A. Rodríguez-Velamazán, O. Fabelo, and M. Braden, *Crystal structure and absence of magnetic order in single-crystalline RuO<sub>2</sub>*, *J. Phys. Condens. Matter* **37**, 135801 (2025).
- [47] S. Brahimi, D. P. Rai, and S. Lounis, *Confinement-induced altermagnetism in RuO<sub>2</sub> thin films*, *arXiv:2412.15377*.
- [48] A. Smolyanyuk, I. I. Mazin, L. Garcia-Gassull, and R. Valentí, *Fragility of the magnetic order in the prototypical altermagnet RuO<sub>2</sub>*, *Phys. Rev. B* **109**, 134424 (2024).



- [49] <https://cstr.cn/31123.02.SECUF>
- [50] G. Beckett, J. Beech-Brandt, K. Leach, Z. Payne, A. Simpson, L. Smith, A. Turner, and A. Whiting, *ARCHER2 service description*, Zenodo, 10.5281/zenodo.14507040, 2024.
- [51] Z. Wu *et al.*, Research data supporting: The Fermi surface of RuO<sub>2</sub> measured by quantum oscillations, Apollo - University of Cambridge Repository, 2025, 10.17863/CAM.119824.
- [52] L. Onsager, *Interpretation of the de Haas–van Alphen effect*, *Philos. Mag.* **43**, 1006 (1952).
- [53] R. B. Dingle, *Some magnetic properties of metals II. The influence of collisions on the magnetic behaviour of large systems*, *Proc. R. Soc. A* **211**, 517 (1952).
- [54] M. Buerger, *The x-ray determination of lattice constants and axial ratios of crystals belonging to the oblique systems*, *Am. Mineral.* **22**, 416 (1937), <https://pubs.geoscienceworld.org/msa/ammin/article-abstract/22/5/416/537857/The-x-ray-determination-of-lattice-constants-and>.
- [55] P. Blaha, K. Schwarz, F. Tran, R. Laskowski, G. K. H. Madsen, and L. D. Marks, *WIEN2K: An APW + lo program for calculating the properties of solids*, *J. Chem. Phys.* **152**, 074101 (2020).
- [56] P. Rourke and S. Julian, *Numerical extraction of de Haas–van Alphen frequencies from calculated band energies*, *Comput. Phys. Commun.* **183**, 324 (2012).
- [57] T. Weinberger, py\_FS, GitHub repository, [https://github.com/TheoWeinberger/py\\_FS](https://github.com/TheoWeinberger/py_FS), 2023.